

This is a repository copy of *New NO<sub>x</sub> and NO<sub>2</sub> vehicle emission curves, and their implications for emissions inventories and air pollution modelling*.

White Rose Research Online URL for this paper:

<https://eprints.whiterose.ac.uk/220209/>

Version: Published Version

---

**Article:**

Stewart, Gregor B., Dajnak, David, Davison, Jack et al. (6 more authors) (2024) New NO<sub>x</sub> and NO<sub>2</sub> vehicle emission curves, and their implications for emissions inventories and air pollution modelling. *Urban Climate*. 102103. ISSN 2212-0955

<https://doi.org/10.1016/j.uclim.2024.102103>

---

**Reuse**

This article is distributed under the terms of the Creative Commons Attribution (CC BY) licence. This licence allows you to distribute, remix, tweak, and build upon the work, even commercially, as long as you credit the authors for the original work. More information and the full terms of the licence here:

<https://creativecommons.org/licenses/>

**Takedown**

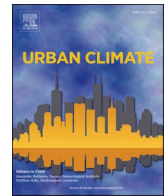
If you consider content in White Rose Research Online to be in breach of UK law, please notify us by emailing [eprints@whiterose.ac.uk](mailto:eprints@whiterose.ac.uk) including the URL of the record and the reason for the withdrawal request.



ELSEVIER

Contents lists available at [ScienceDirect](https://www.sciencedirect.com)

## Urban Climate

journal homepage: [www.elsevier.com/locate/uclim](http://www.elsevier.com/locate/uclim)

## New NO<sub>x</sub> and NO<sub>2</sub> vehicle emission curves, and their implications for emissions inventories and air pollution modelling

Gregor B. Stewart<sup>a,b</sup>, David Dajnak<sup>a,b,\*</sup>, Jack Davison<sup>d,e</sup>, David C. Carslaw<sup>d,e</sup>, Andrew V. Beddows<sup>a,b</sup>, Napameth Phantawesak<sup>f</sup>, Marc E.J. Stettler<sup>f</sup>, Michael J. Hollaway<sup>g</sup>, Sean D. BeEVERS<sup>a,b,c</sup>

<sup>a</sup> Environmental Research Group, School of Public Health, Imperial College London, Michael Uren Biomedical Engineering Hub, White City Campus, Wood Lane, London W12 0BZ, UK

<sup>b</sup> MRC Centre for Environment and Health, Imperial College London, UK

<sup>c</sup> NIHR HPRU in Environmental Exposures and Health, Imperial College London, UK

<sup>d</sup> Wolfson Atmospheric Chemistry Laboratories, University of York, York YO10 5DD, UK

<sup>e</sup> Ricardo Energy & Environment, Harwell, Oxfordshire OX11 0QR, UK

<sup>f</sup> Department of Civil and Environmental Engineering, Imperial College London, South Kensington Campus, London SW7 2AZ, UK

<sup>g</sup> UK Centre for Ecology and Hydrology, Lancaster Environment Centre, Lancaster, UK

## ARTICLE INFO

## Keywords:

Remote sensing  
Emission factors  
Urban air pollution

## ABSTRACT

Emissions of NO<sub>x</sub> and primary NO<sub>2</sub> from road transport sources are highly influential in NO<sub>2</sub> exposure at both local and regional scales; quantifying these accurately is therefore an important but challenging component of emissions inventory and air pollution model development. Results are presented from an urban air pollution model, after creation of new speed-emissions curves for NO<sub>x</sub> through the combination of available vehicle drive cycles and nearly 500,000 UK-based remote sensing measurements of exhaust emissions. Vehicle power-based relationships are applied to 1 Hz drive cycle datasets, with random sampling of the outputs allowing generation of the new curves. These demonstrate significantly higher emissions than those predicted by existing curves for most Euro VI HGVs, and among successive petrol and diesel passenger cars; this may be partly explained by relatively low UK ambient temperatures, as well as an underestimation of the level of tampering with HGV SCR systems. Implementation of the curves in a detailed emissions inventory for London, UK in 2019 leads to substantially improved air pollution model performance for NO<sub>x</sub>/NO<sub>2</sub>; normalised mean bias reduces in magnitude, changing from  $-0.18$  to  $+0.01$  for NO<sub>x</sub> and  $-0.12$  to  $+0.01$  for NO<sub>2</sub>. The curves developed are widely applicable, and the novel approach outlined has the potential to improve source apportionment and future model predictions under differing policy scenarios, produce better exposure estimates for health-related studies and revise NO<sub>x</sub> emissions budgets for compliance with the NEC Directive, all of which are important for the development of mitigation policies.

\* Corresponding author at: Environmental Research Group, School of Public Health, Imperial College London, Michael Uren Biomedical Engineering Hub, White City Campus, Wood Lane, London W12 0BZ, UK.

E-mail address: [d.dajnak@imperial.ac.uk](mailto:d.dajnak@imperial.ac.uk) (D. Dajnak).

<https://doi.org/10.1016/j.uclim.2024.102103>

Received 4 April 2024; Received in revised form 19 July 2024; Accepted 10 August 2024

Available online 20 August 2024

2212-0955/© 2024 The Authors. Published by Elsevier B.V. This is an open access article under the CC BY license (<http://creativecommons.org/licenses/by/4.0/>).

## 1. Introduction

Emissions inventories are a critical tool for policymakers and modellers in determining the effectiveness of intervention measures on reducing air pollution, as well as the relative contributions of different sources to air pollutant concentrations at specific locations.

Despite the introduction of control technologies and implementation of successive emissions standards, road transport remains a major contributor to emissions of nitrogen oxides (NO<sub>x</sub>) across Europe, with 37% of NO<sub>x</sub> emissions coming from this sector across the EU-27 in 2020 (European Environment Agency, 2022). In heavily populated urban environments, the figure can be higher, with 44% of NO<sub>x</sub> emissions in London in 2019 coming from the road transport sector, according to calculations made using existing emissions factors (Greater London Authority, 2021). At roadside locations in many cities across Europe, EU legal limits on annual mean nitrogen dioxide (NO<sub>2</sub>) concentrations continue to be exceeded, and in the year 2022, 90% of the EU urban population was exposed to annual average NO<sub>2</sub> concentrations above the World Health Organization (WHO) guideline of 10 µg m<sup>-3</sup> (European Environment Agency, 2023). Local emissions of NO<sub>x</sub> from road traffic, both as NO and NO<sub>2</sub>, are and have historically been the main drivers of such exceedances (European Environment Agency, 2022; Casquero-Vera et al., 2019). These emissions have a further role in that NO<sub>x</sub> is an important precursor for fine particulate matter at a regional level (Clappier et al., 2021; Beekmann et al., 2015). Road transport NO<sub>x</sub> emissions rates, including the proportion of NO<sub>x</sub> emitted directly as NO<sub>2</sub> (f-NO<sub>2</sub>), are therefore important to quantify accurately.

In fine-scale urban air quality models, it is necessary to quantify emissions rates from specific road sources. Speed-emissions curves are used routinely in emissions inventories to estimate exhaust emissions of air pollutants (Garland et al., 2022); despite the relatively poor association between average speed and the emissions rate of a vehicle, other metrics which are better predictors, such as vehicle-specific power (Carslaw et al., 2013), are not typically available across a road network. It therefore remains necessary to create and apply speed-emissions curves to produce as accurate as possible a road transport emissions inventory.

In recent years, European emissions factors have often underestimated the contribution of road transport sources to NO<sub>2</sub> concentrations in urban areas (Lewis et al., 2015). When base year emissions inventories require scaling factors for road transport emissions to correct for bias at roadside monitoring sites, projecting future concentrations using the same scaling factors potentially creates a large systematic error, as older vehicles which contribute to the scaling factors required are phased out of the fleet.

The European Monitoring and Evaluation Program (EMEP)/European Environment Agency (EEA) Emission Inventory Guidebook recommends the use of COPERT (Computer Program to calculate Emissions from Road Transport) emissions curves, which many European emissions inventories rely on, including the UK National Atmospheric Emissions Inventory (NAEI) (National Atmospheric Emissions Inventory, 2022; Emisia, 2023; Ntziachristos and Samaras, 2023). The emissions factors used for heavy-duty vehicles (HGVs, buses and coaches) are taken from the Handbook Emission Factors for Road Transport (HBEFA) (Notter et al., 2022). Speed-emissions curves are generated from a European database of emissions tests, which now includes portable emissions measurement systems (PEMS) data gathered from on-road measurement campaigns as well as chassis dynamometer laboratory studies over real-world drive cycles (Emisia, 2023; Ntziachristos and Samaras, 2023; Murrells and Rose, 2019). PEMS instruments provide detailed data across an entire drive cycle for the vehicle in question, and a number of studies have demonstrated their capability (O'Driscoll et al., 2016; O'Driscoll et al., 2018; Bishop et al., 2019; Zheng et al., 2021; Söderena et al., 2020). However, the practicalities of this approach, in terms of cost and time, mean that the sample size of vehicles monitored is relatively small.

A number of studies have demonstrated the use of remote sensing devices (RSD) in measuring pollutants from vehicle exhausts (Carslaw et al., 2011; Carslaw and Rhys-Tyler, 2013; Chen and Borken-Kleefeld, 2016). An advantage of RSD over PEMS is the ability to measure emissions from vast quantities of vehicles, therefore giving a more reliable sample of the fleet, and the implicit inclusion of any effects of vehicle deterioration on emissions, an influence that is typically treated separately in commonly used emissions factors such as COPERT.

We make use of recent real-world measurements made by remote sensing devices, and relationships derived from these data, to relate vehicle power to emissions rates. The new relationships are applied to drive cycle data from a suite of light-duty and heavy-duty vehicles in an urban environment, allowing the generation of new speed-emissions curves for NO<sub>x</sub>, and processing of the data through a well-established, long-used and accepted emissions inventory tool and urban air quality model, the London Toolkit, referred to elsewhere as *KCLurban* (Beever et al., 2013). The model, which has historically followed EMEP/EEA guidebook recommendations, as is standard throughout Europe, is evaluated against measured data in 2019, both with and without the incorporation of the new emissions factors for NO<sub>x</sub>/NO<sub>2</sub>, and the performance compared between the two runs. The aim is to demonstrate the applicability of the new methods for air pollution modelling. The new speed-emissions curves are hereafter referred to as DUKEMS curves, relating to the UK research project which this work was a part of. The project aim was to improve emissions databases in the UK more generally, across a wide range of sources and pollutants, thereby enabling improved air pollution modelling.

## 2. Methods

### 2.1. Vehicle emission remote sensing data

The analysis makes use of extensive vehicle emission remote sensing data that has been collected over the period 2017 to 2022 throughout the UK, augmenting the measurements of Davison et al. (2021) with more recent data, measurements from heavy-duty vehicles and from newer vehicle technologies (Davison et al., 2021). Measurements were undertaken using the Fuel Efficiency Automobile Test (FEAT) instrument developed by the University of Denver and the commercially available Opus AccuScan RSD 4600/5000. This uses open path spectroscopy to measure the exhaust gases from each passing vehicle, using UV and IR sources and multiple detectors to achieve this. The instrument also includes a laser-based method to measure speed and acceleration, and a camera to

capture vehicle number plates. The technique is described in further detail elsewhere (Bishop and Stedman, 1996; Burgard et al., 2006).

In this study, 498,891 valid NO<sub>x</sub> measurements of individual vehicles have been used as the basis for emission factor calculation. The measurements span a wide range of locations (49 unique locations in 15 cities throughout the UK) and ambient conditions. The ambient temperature conditions spanned  $-1\text{ }^{\circ}\text{C}$  to  $29\text{ }^{\circ}\text{C}$  with a mean of  $13.8\text{ }^{\circ}\text{C}$ , typical of meteorological conditions experienced in the UK. The specific sizes and Euro standards of vehicles covered by remote sensing data, including passenger cars, light goods vehicles (LGVs), buses, heavy goods vehicles (HGVs) and London taxis, are detailed in the supplementary material.

Fundamentally, remote sensing instruments measure ratios of pollutant gases as a ratio to CO<sub>2</sub>, from which it is possible with some basic fuel composition and combustion assumptions to derive fuel-based emission factors, e.g. grams of NO<sub>x</sub> per kg of fuel. However, to calculate emissions as expressed in speed-emission curves it is necessary to derive emission factors expressed in g/s or g/km. The essential step required for this calculation is the estimate of fuel consumption at the time a measurement is made. The physics-based approach used to derive relationships between vehicle specific power (VSP) and emissions rates is described in detail elsewhere, but is summarised here (Davison et al., 2020).

To calculate NO<sub>x</sub> emissions rate for each vehicle measurement, an estimate must be derived of instantaneous fuel consumption, using VSP. Instantaneous vehicle power is calculated initially as the total power required to overcome air and rolling resistance, road gradient, a vehicle's acceleration and the power required for auxiliary devices and losses in transmission, which are also accounted for. Assumptions are made on the vehicle mass and aerodynamic drag coefficients, using generic values (Davison et al., 2020). VSP is then derived by dividing the instantaneous power by vehicle mass, having accounted for weight of passengers and cargo. Fuel consumption is calculated using VSP through the Passenger Car and Heavy Duty Emission Model (PHEM) (Hausberger, 2003). These calculations provide an estimate of fuel consumption in g/s. Relationships can therefore be derived between emissions rates in g/s for each pollutant measured and VSP, across each desired subset of vehicles. The final step is to apply the predictions of g/s emissions to modal (1 Hz) drive cycles, such as those from PEMS measurements, to generate a time series of emissions expressed in g/s, which can also be used to calculate emission factors in g/km over a wide range of conditions.

## 2.2. Drive cycle data

Appropriate 1 Hz drive cycle datasets were required in order to represent speed and acceleration/deceleration under real driving conditions for different types of vehicle across varying road types and road gradients. For passenger cars and vans, 55 drive cycles were used based on extensive vehicle PEMS measurements conducted by the UK Department for Transport. The drive cycles covered urban, rural and motorway driving; an example is shown in the supplementary material. In total, these drive cycles covered over 4200 km of real driving (Davison et al., 2021).

Specific London bus and taxi drive cycles developed between TfL and Millbrook were used for these vehicles. Test cycles for heavy goods vehicles (HGVs) and coaches were provided by the Energy Saving Trust, Zemo and TfL, and were based on those developed between TfL and Millbrook, with additional sections added for higher speeds for coaches and HGVs. The test cycles therefore covered driving conditions on city-centre, urban and extra-urban roads.

The speed trace over the London bus cycle is shown in Fig. 1, with further information on each drive cycle available in the supplementary material.

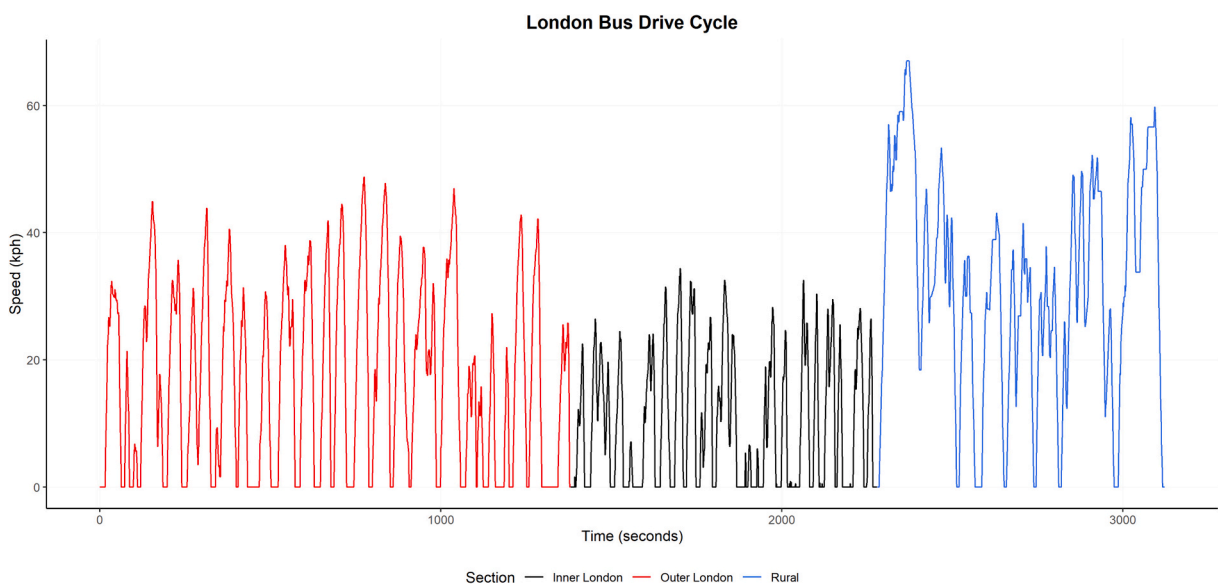


Fig. 1. Drive cycle data used for London buses. The trace shows the speed of the bus over the duration of the cycle.

### 2.3. Creation of new speed-emissions curves

The data were further processed as follows. Within the existing London emissions tool, for the region of London (Urban/Suburban/Motorway) appropriate to the drive cycle section, an average transit time, in seconds, across an Ordnance Survey (OS) Topographic Identifier (TOID) link was calculated (Ordnance Survey, 2023). The OS TOID link is the level at which speeds and traffic flows can be specified in the London emissions tool, and on which the tool generates bottom-up emissions calculations using local vehicle fleet compositions. These transit times were used to sample randomly 500 times for each vehicle type's corresponding drive cycle. In each of the random samples, an average speed (kph) and emission rate (g/s) was generated. Units of g/s, rather than g/km, were used since at very low speeds, the g/km curves tend to infinity, making model fitting more difficult (Davison et al., 2021).

The resulting datasets were used to fit a generalised additive model (GAM) for each vehicle and pollutant, aggregated over all road types, relating average speed to emission rate. The *mgcv* R package was used with the restricted maximum likelihood (REML) method (Wood, 2017). The maximum allowed value of  $k$ , which places an upper limit on the effective degrees of freedom in the smooth function, was set to 6, given prior knowledge about the form of the curves expected from COPERT data, and to avoid overfitting. One exception was for the Euro VI hybrid double decker London bus, where use of  $k = 6$  caused the curve to be overfitted; the value was therefore set at 4.

Primary NO<sub>2</sub> emissions were calculated by applying up-to-date f-NO<sub>2</sub> values to both sets of NO<sub>x</sub> curves. These were provided through analysis of the same set of remote sensing data and are presented in the supplementary material.

#### 2.3.1. Additional assumptions

The remote sensing measurements explicitly do not include hybrid light-duty gasoline vehicles under battery operation; therefore, scaling factors were applied to the new curves for the equivalent internal combustion engine (ICE) vehicles; standard hybrid emissions were revised downward by 23% and plug-in hybrids by 41%, in line with the respective utility factors calculated over all driving conditions by Farren et al. (Farren et al., 2020).

Speed-dependent utility factors were applied to hybrid Euro VI double-decker London buses using data from Phantawesak et al. (Phantawesak et al., 2022), which allowed calculation of the proportion of engine-off time spent by both parallel and series hybrid Euro V buses. Further detail on this method is provided in the supplementary material.

Where data existed on a given Euro standard, size and technology for both London-specific and non-London urban buses, the curves generated for the London buses were used in preference. The curves produced from both sets of data are, however, presented in the results.

Vehicles retrofitted with control technologies, and the relative proportions of Euro V vehicles with an EGR or SCR system, were assumed to have been accounted for in the initial measurement campaign; as such, the same curves were applied to all vehicles within a given class, Euro standard, size range and engine technology.

There was only a sufficient sample size from the medium size class (1.4–2.0 l) of Euro 6-d diesel cars. The curves fitted for this vehicle were therefore also used for the small (< 1.4 l) and large (> 2.0 l) size classes. However, post-Euro 6c vehicles represented <1% of cars and LGVs in the London fleet in 2019, so this had minimal impact on the model as a whole.

### 2.4. London Atmospheric Emissions Inventory 2019

The London Atmospheric Emissions Inventory (LAEI) 2019 (Greater London Authority, 2021) formed the basis for the implementation of new emissions curves. The most recent version was carried out for the year 2019, during which an Ultra Low Emission Zone (ULEZ) was implemented in Central London on 8th April, covering the same area as the Congestion Charging Zone, but prior to further expansions of the ULEZ to all of Inner London and subsequently Outer London, which took place in October 2021 and August 2023 respectively.

The LAEI2019 provided average speed data, as well as detailed traffic flows for specific groups of vehicles, on nearly 80,000 major road segments by annual average hour of the day. The road geographies were derived from Ordnance Survey's (OS) Integrated Transport Network (ITN), with the segments each having an OS TOID (Ordnance Survey, 2023). Combined with zonal fleet compositions and COPERT speed-emissions factors, this allowed emissions to be estimated on individual major roads throughout London. Fleet compositions did not include estimations of the proportions of Euro 6d-temp diesel light-duty vehicles in 2019. The emissions factors used in the LAEI2019 were from COPERT v5.0; these were upgraded to v5.7 (Emisia, 2023; Ntziachristos and Samaras, 2023), the latest provided at the time of writing, for the comparisons in this study. Further detail on a minor update of LAEI speed data is included in the supplementary material.

Minor road vehicle emissions were calculated using LAEI vehicle km estimates by km<sup>2</sup> grid cell and distributed on minor roads from the ITN accordingly (Greater London Authority, 2021). Additional NO<sub>x</sub> emissions from cold starts in light-duty vehicles are also accounted for according to EMEP guidebook recommendations (European Environment Agency, 2019), based on estimations of light-duty vehicle starts in the LAEI. These emissions were distributed as area sources on a km<sup>2</sup> basis (Greater London Authority, 2021).

Non-road sources' emissions used in all model runs were entirely consistent with the LAEI2019; these included industrial point sources, aviation, shipping, domestic and commercial combustion from gas and other fuels, rail, commercial cooking, domestic wood burning and construction sources (Greater London Authority, 2021). More detail on the setup of these sources in the model is given in section 2.6.

## 2.5. COPERT emissions factors

COPERT v5.7 included estimates of cold emissions rates from heavy vehicles, which were implemented for the first time in v5.6 (Emisia, 2023; Ntziachristos and Samaras, 2023). Given the proportion of heavy-duty vehicle mileage on major roads, and the 8.5 km at the start of each trip estimated by COPERT to be under cold engine conditions, cold emissions rates for HDVs were added to the hot emissions rates across all roads. Owing to the difficulty in estimating average trip lengths for HDVs in London, and the congested conditions, it was assumed that heavy vehicles moved under cold operating conditions 100% of the time. This therefore maximised the emissions that could be calculated from these functions. Extra emissions were not added above 45 kph, this being the limit of the cold emission functions provided through COPERT.

The COPERT curves used in this analysis also include up-to-date fuel and degradation scaling factors up to the year 2019, the latter calculated using average mileage statistics from the UK Department for Transport by vehicle Euro standard and size (National Atmospheric Emissions Inventory, 2022; Department for Transport, 2009). HGV and bus speed-emissions functions were those with the road slope set to 0% and the vehicle load percentage to 50%.

## 2.6. London Toolkit

The London Toolkit is the model of choice in assessing the impacts of London policies on air pollution, having been used in the LAEI for over two decades, as well as in development of policies such as the Congestion Charging Zone and Ultra Low Emission Zone. It uses a kernel modelling approach to describe the dispersion from the sources incorporated into the emissions inventory, with an empirical approach, based on prior measurements of  $\text{NO}_x$  and  $\text{NO}_2$  at background and roadside sites, used to calculate annual mean  $\text{NO}_2$  concentrations. This follows the established methodology of Carslaw et al., applied to observations from 2019, and accounts for the dispersion of primary  $\text{NO}_2$  emissions (Carslaw et al., 2001). The model is detailed briefly here, but is described in further detail by Beevers et al. and Kelly et al., referred to as *KCLurban* (Beevers et al., 2013; Kelly et al., 2011).

The regional contribution to  $\text{NO}_x$  concentrations, of  $10.3 \mu\text{g m}^{-3}$  in 2019, was calculated using the US EPA CMAQ chemical transport model (United States Environmental Protection Agency, 2022; Byun and Schere, 2006). This was run in the same way as outlined by Dajnak et al., for the year 2019 in this instance (Dajnak et al., 2023). The value used for the regional contribution corresponded to the lowest concentration predicted in any  $2 \text{ km} \times 2 \text{ km}$  grid in a 20 km zone around the M25 orbital motorway. Dispersion kernels for the toolkit model were created with ADMS 5 or ADMS-Roads (Cambridge Environmental Research Consultants, 2016; Cambridge Environmental Research Consultants, 2020) for each source type, using hourly meteorological data for 2019 from London Heathrow airport and a unit source strength of  $1 \text{ g/s}$  (point and jet sources),  $1 \text{ g m}^{-3} \text{ s}^{-1}$  (volume sources) or  $1 \text{ g km}^{-1} \text{ s}^{-1}$  (road sources) (Carslaw, 2023). The hourly meteorological data, which were recorded at a height of 10 m, included measurements of wind speed, wind direction, temperature, relative humidity, precipitation and cloud cover. Surface roughness at the meteorological station was assumed to be 0.2 m, with a value of 1.5 m assumed at dispersion sites, as recommended for large urban areas. The minimum Monin-Obukhov length required by ADMS was set at 100 m, again as recommended for large urban conurbations. These input parameters allow estimation of boundary layer height, which in turn contributes to the parameterisation of the boundary layer structure in the creation of each kernel (Cambridge Environmental Research Consultants, 2016; Cambridge Environmental Research Consultants, 2020).

Contributions from each source were summed onto a  $20 \text{ m} \times 20 \text{ m}$  horizontal grid, having adjusted for the relevant source strength. At distances of over 500 m from a receptor, sources were represented as shallow volumes of  $1 \text{ km} \times 1 \text{ km}$  horizontally, 2 m deep for sources below that height and 50 m deep for others.

Within 500 m of receptors, road, rail, airport, gas combustion and shipping sources were treated in a more detailed way as explained below. Emissions on roads were represented as a series of 10 m-long road links, totalling approximately 2.4 million road sources up to and including the M25 ring road. Major road source kernels in London were classified into 217 types of road, according to street orientation, building height, street and road width within the ADMS-Roads Advanced Street Canyon Module (Cambridge Environmental Research Consultants, 2020).

Gas combustion, also a substantial source of  $\text{NO}_x$  in London, was represented spatially using points located at 50 m intervals throughout the minor road network and set back 20 m from the road. Separate dispersion kernels were created to release emissions at heights of 1 m (domestic), 30 m (small commercial premises) and 75 m (large commercial premises) with various release conditions, and diurnal and monthly emissions profiles derived from UK gas use statistics. (UK Department for Energy Security and Net Zero and UK Department for Business Energy and Industrial Strategy, 2024)

Railway sources were treated similarly to roads but with a release height of 5 m, with the network split into 10 m sections. Aircraft sources were accounted for in detail at Heathrow Airport during approach, landing, taxiing, take off, initial climb and climb out. This was also done using individual sources 10 m apart. Accelerating aircraft were modelled as stationary jet sources, from the location of the start of ground-roll to the point at which the aircraft left the ground. The emissions were assumed to have a decreasing effect on ground-level concentrations with increasing height. Auxiliary power unit (APU) and engine testing emissions were represented as stationary point sources.

Shipping emission dispersion was represented using four aggregated categories of vessel, with release heights of 5 m, 17.5 m, 30 m and 50 m. The emissions were released along the Thames river at a series of points separated by 20 m, having originally incorporated activity data provided by the Port of London Authority (PLA) in 2016, and scaled this to 2019 (Aether Ltd, 2017; Port of London Authority, 2022).

Dispersion from large industrial sources was modelled using specific release conditions, including height, temperature and volume

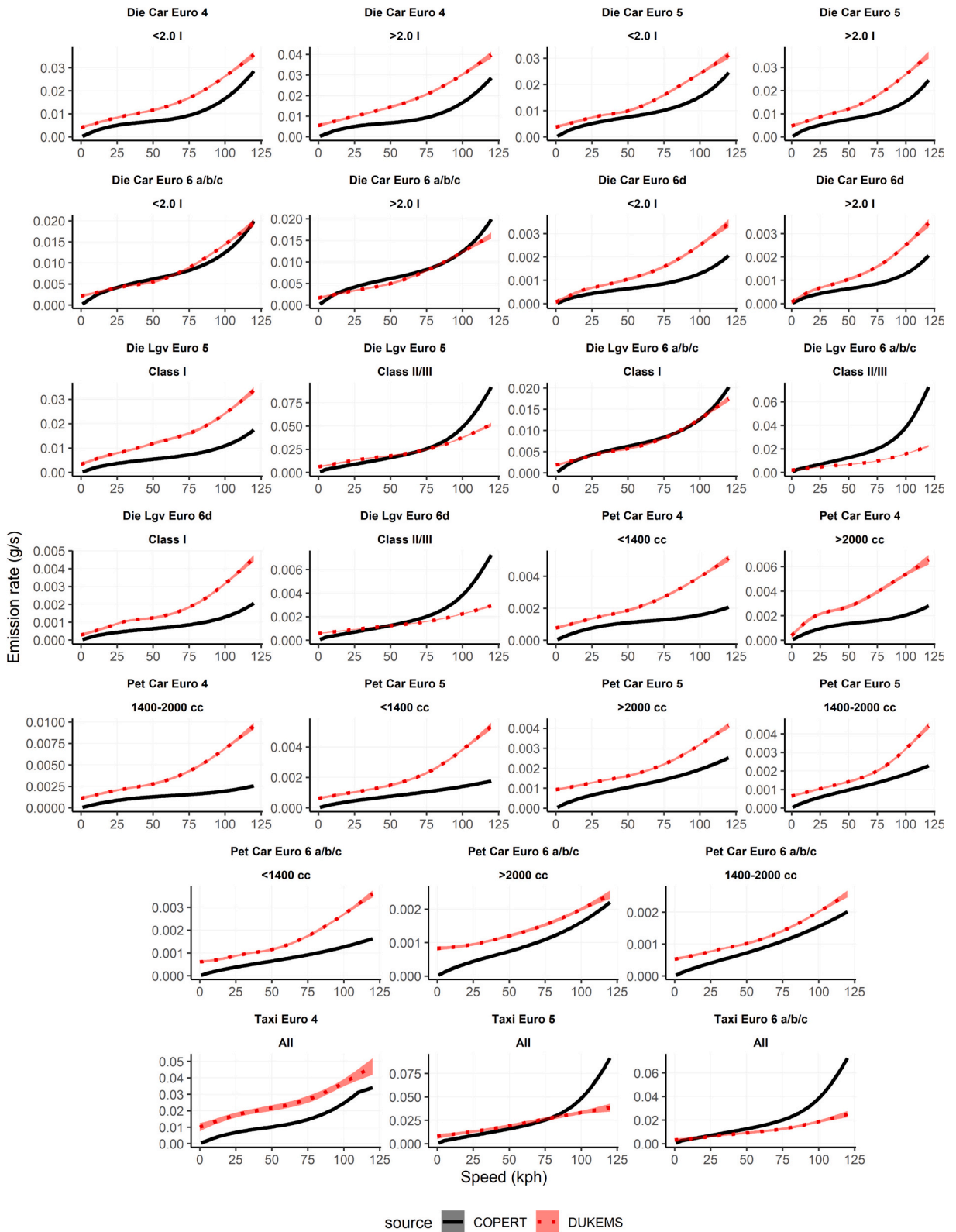


**Fig. 2.** Newly created NO<sub>x</sub> speed-emissions curves for light-duty ICE vehicles, alongside those from COPERT. The plot is faceted by vehicle group, fuel type, Euro standard and size classification.

flow rate. Further information on the treatment of other source types is described in detail by Beevers et al. (Beevers et al., 2012).

The model produces ground-level annual average concentrations of NO<sub>x</sub> and NO<sub>2</sub> at 20 m horizontal resolution, allowing evaluation against 121 fixed-site monitors across the London Air Quality Network (LAQN), Heathrow Airwatch and Air Quality England air quality networks (Imperial College London, 2023; Ricardo Energy and Environment, 2023; Heathrow Airport Ltd, 2023). Monitoring stations in 2019 included 63 roadside, 12 kerbside, 39 background and 7 industrial sites. Concentrations at roadside and kerbside sites specifically were modelled at 5 m resolution to better represent the concentration gradient resulting from dispersion of road transport emissions.

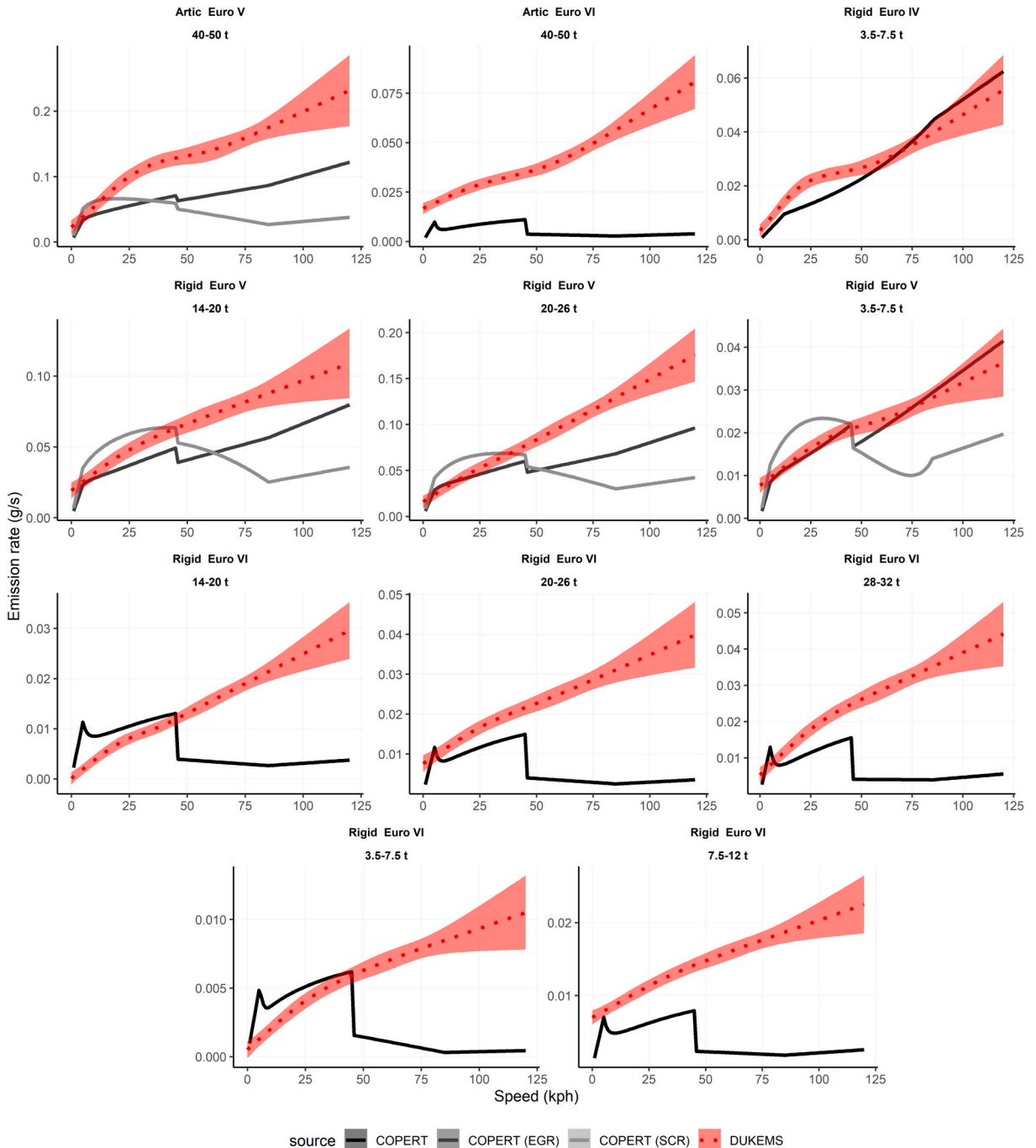


**Fig. 3.** Newly created NO<sub>x</sub> speed-emissions curves for heavy goods vehicles, alongside those from COPERT. The plot is faceted by vehicle group, Euro standard and size classification. Euro V curves (an aggregate of all Euro V vehicles measured) are compared to those of both EGR and SCR vehicles from COPERT.

2.7. Road emissions coverage

The vehicles covered by new emissions factors accounted for 75.5% and 79.3% of NO<sub>x</sub> and primary NO<sub>2</sub> emissions respectively in the LAEI2019, calculated using the updated COPERT factors. Sufficient measurements were not available for motorcycles, coaches or petrol LGVs, and new curves for these were therefore not created. Along with the other remaining vehicles, their emissions continued to be estimated with COPERT curves in the updated model run.

3. Results

The hot emissions curves generated are compared in this section to the corresponding COPERT v5.7 functions made available in the EMEP Guidebook at the time of writing. Before generating the figures presented, petrol cars with failed catalytic converters were accounted for according to the proportion of these in each successive Euro standard in London in the LAEI2019; revised curves were produced accordingly (Greater London Authority, 2021). Euro 6 diesel cars with a failed SCR system were accounted for analogously.

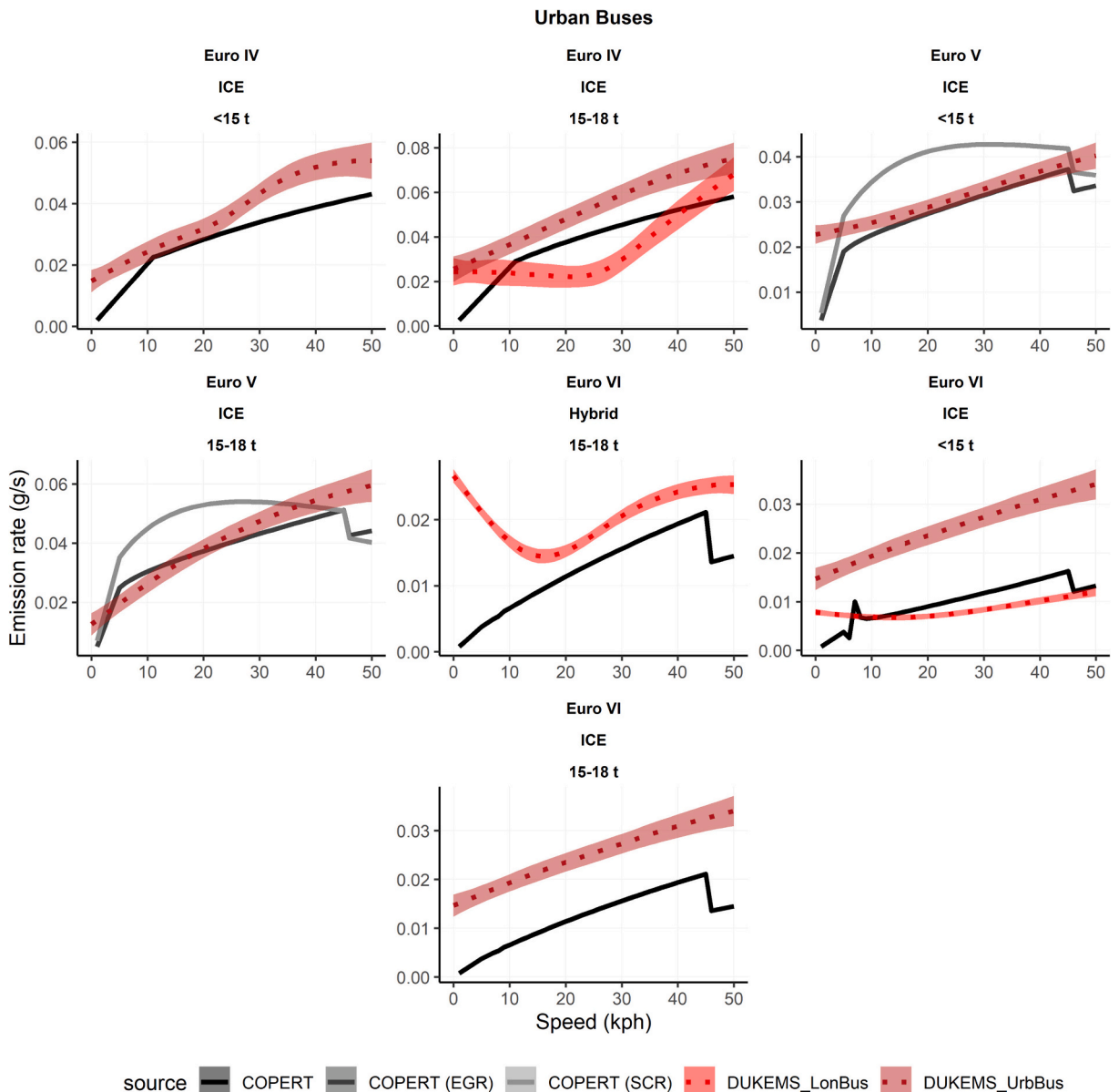


Fig. 4. Newly created NO<sub>x</sub> speed-emissions curves for urban buses and London-specific buses, alongside those from COPERT. The plot is faceted by vehicle group, Euro standard and size classification. Euro V curves (an aggregate of all Euro V vehicles measured) are compared to those of both EGR and SCR vehicles from COPERT.

COPERT figures used for heavy vehicles in the comparison included the additional emissions predicted under cold operating conditions. The new curves produced are shown alongside those from COPERT through Fig. 2 to Fig. 4, across all speeds used in the model; the shading around each DUKEMS curve represents the 95% confidence interval. Although pre-Euro 4/IV vehicles' emissions were updated in the model, for clarity they are omitted from the figures presented. Because of discontinuities in assumptions regarding cold emissions and capping of g/km rates above and below certain speeds, the COPERT functions are presented as line plots through each integer speed value rather than smooth curves.

Differences between the new emissions curves and the corresponding COPERT curves, with units converted to g/km, are shown in Fig. 5, at three different speeds typical of urban, suburban and motorway driving respectively, with the upper and lower bounds of the 95% confidence interval in each GAM fit also converted to g/km and shown by the vertical lines. The data presented in Fig. 6 show the impact of the new curves on the emissions, in tonnes across the modelled area in 2019; these impacts are broken down by vehicle subgroup and Euro standard. The larger contribution of Euro 5/6 vehicles to these discrepancies is in part owing to the relatively higher proportions of these in the fleet in 2019, compared to earlier Euro standards.

### 3.1. Light-duty vehicle emissions

New curves for Euro 6 a/b/c diesel cars show comparable NO<sub>x</sub> emissions rates to COPERT across the majority of the speed range. In the Euro 6-d phase, the new curves exceed those from COPERT across the whole speed range. Although the number of these vehicles present in 2019 was small (< 1% of cars and LGVs) and the impacts on emissions are therefore negligible, as shown in Fig. 6, the discrepancies will become more apparent when future year model runs are undertaken. Despite these discrepancies, the curves produced for Euro 6-d diesel cars confirm the improvement relative to previous Euro standards, including the initial phases of Euro 6, and indeed to equivalent petrol cars at the typical urban speed; this is shown in the supplementary material. Petrol cars' NO<sub>x</sub> emissions from Euro 4 onwards are shown to exceed those predicted by COPERT across all speeds, although these are still substantially lower than all but the most recent phase of Euro 6 diesel.

There is a more complex picture for diesel LGVs, where the new curves predict substantially lower NO<sub>x</sub> emissions from Euro 6 a/b/c Class II/III vehicles than COPERT. This is also the case at the typical rural and motorway speeds for the Euro 5 and Euro 6-d Class II/III diesel LGVs. The new curves for smaller diesel LGVs (Class I), which make up a significantly smaller proportion of the fleet, are comparable to COPERT for Euro 6 a/b/c, but exceed COPERT for Euro 5 and Euro 6-d.

While the discrepancies, both in terms of absolute g/km difference and ratio to COPERT, are smaller than many of those observed in certain categories of HGV and bus, the substantially larger contribution of light-duty vehicles to overall vehicle mileage in an urban area means the changes to their emissions curves have more of an impact on the model, as shown in Fig. 6.

### 3.2. Heavy-duty vehicle emissions

Some wide discrepancies between the new speed-emissions curves and those from COPERT are notable from Figs. 3 to 5. The largest absolute discrepancies across all example speeds are seen for Euro V articulated HGVs. However, given the high proportion of Euro VI articulated HGVs already in the fleet in 2019, the discrepancies for Euro VI articulated HGVs have a larger impact on the emissions calculated in 2019, as shown in Fig. 6.

At the typical urban speed of 35 kph, the Euro VI 40–50 t articulated HGV exceeds the COPERT emissions rate by a factor of 3.2; the

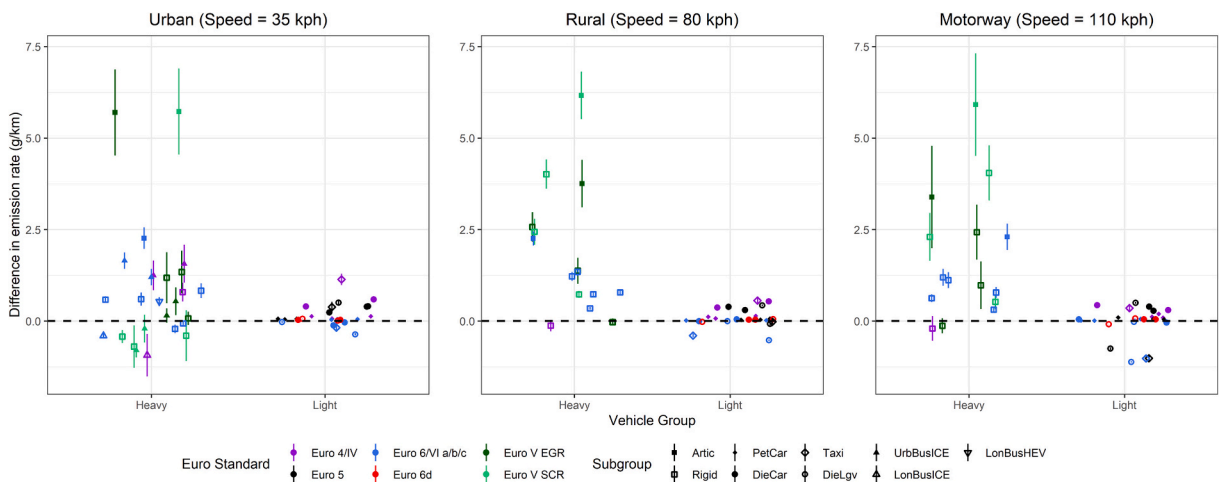
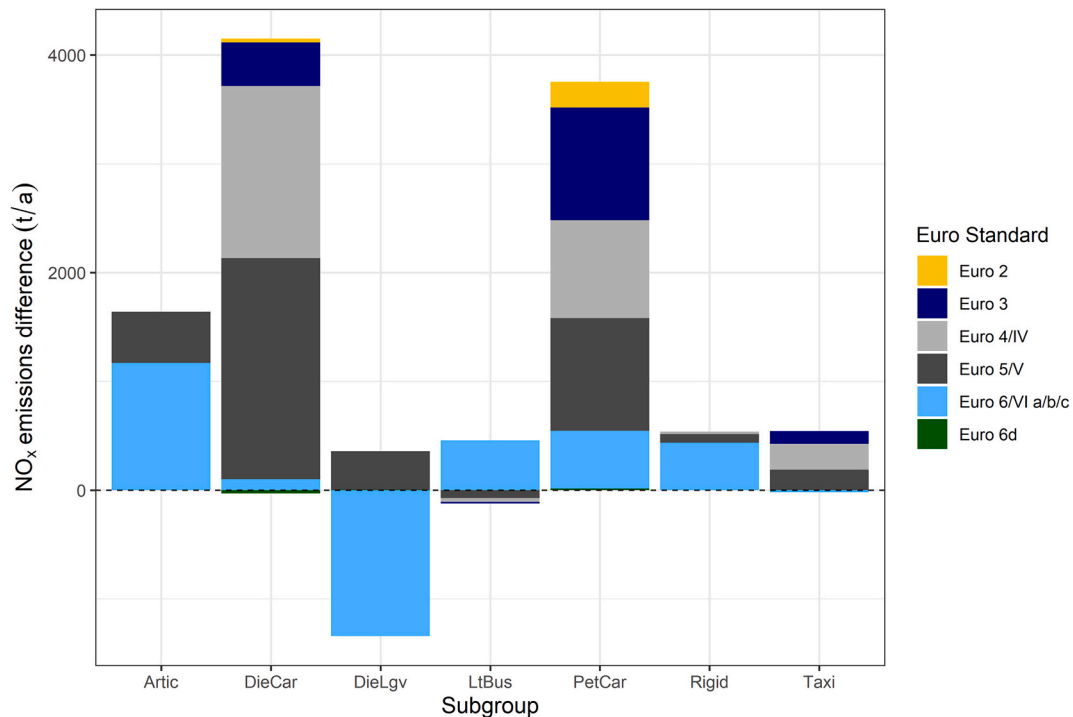


Fig. 5. Differences between new emissions curves and COPERT functions at typical speeds representing Urban, Rural and Motorway driving. The data are transformed to units of g/km for this comparison and are colored by Euro emissions standard. The 95% confidence interval in the GAM fit for each vehicle, also converted from g/s to g/km, is represented by the vertical lines – in some cases, these are too small to be clearly visible. Positive values indicate higher values for the new curves.



**Fig. 6.** Difference in overall vehicle NO<sub>x</sub> emissions in 2019 (tonnes per annum) upon adoption of the new speed-emissions curves. Data are split by vehicle type and Euro standard, and represent the area up to and including the M25 orbital motorway. Positive values indicate higher emissions from the new curves.

rigid HGV Euro VI vehicles exceed the COPERT emissions rate in three size classes (7.5–12, 20–26 & 28–32 t), by up to a factor of 1.8, but lower emissions rates are predicted in another two size classes (3.5–7.5 & 14–20 t). The rigid HGV plots within Fig. 3 show that some of the size classes demonstrate reasonably close agreement at lower urban speeds, when cold emissions rates are applied to any movement of the vehicles under 45 kph. Mixed results are also observed for London buses: at the typical urban speed the new curves give lower (ratio = 0.7) NO<sub>x</sub> emissions than COPERT for the single-decker Euro VI bus, but higher emissions for the hybrid double-decker bus (ratio = 1.3) which, given its prevalence in the fleet, has a larger impact on emissions in London.

At the typical rural and motorway speeds of 80 and 110 kph respectively, large absolute discrepancies in g/km are observed among HGVs. The ratios to COPERT are particularly high among Euro VI vehicles, reaching as high as 18.6 at 80 kph and 24.6 at 110 kph. The comparison is not made for London buses other than at the urban speeds, since these vehicles do not typically travel at the higher average speeds used to compare on rural roads and motorways. A greater degree of uncertainty exists in the data provided by the remote sensing measurements, and therefore in the curves generated, at speeds above 80 kph, given the lack of remote sensing measurements made at these speeds; this uncertainty is explored further below.

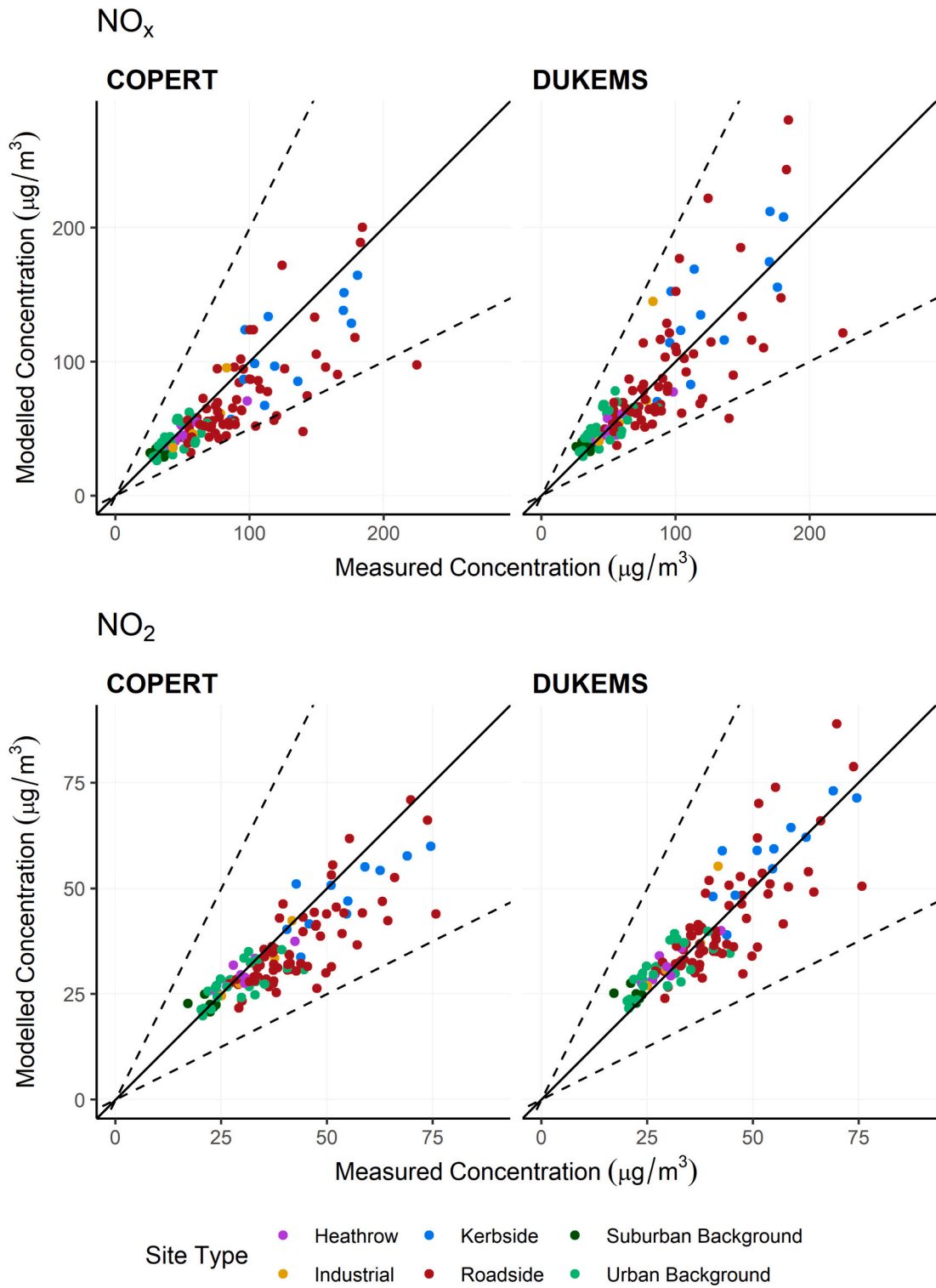
### 3.3. Emissions impact and sensitivity

Table 1 shows the change in emissions by geographical zone in London upon adoption of the DUKEMS speed-emissions curves. The zones are mutually exclusive and represent the same zones used to represent vehicle fleet compositions in the LAEI; the areas they cover are illustrated in the supplementary material.

There is an increase of 9.4 kt (36%) of NO<sub>x</sub> emissions throughout the modelled area, and a 1.2 kt (31%) increase in emissions of primary NO<sub>2</sub>, with the largest relative changes seen in more central areas; this is predominantly because of large relative discrepancies between the two sets of functions at the very low average speeds often observed in more congested areas.

There is a greater degree of uncertainty in the data provided by the remote sensing measurements of HGVs, and therefore in the curves generated, at speeds above 80 kph. To evaluate the impact of this uncertainty, a separate emissions model was run using COPERT functions for these vehicles on road links with annual average speeds exceeding 80 kph. The results of this sensitivity test, relative to the run with DUKEMS curves used everywhere, are also presented in Table 1.

The results show a minimal impact on most zones within London and a 4% decrease in NO<sub>x</sub> emissions overall relative to using the new curves everywhere. The largest impacts are on motorways, as shown by the effects on emissions on the M25. However, given the lack of monitoring sites located next to motorways and the slower average speeds observed throughout most of a densely populated urban area such as London, the impacts on the air pollution model evaluation are likely to be very small.



**Fig. 7.** Scatter plots illustrating the relationship between measured and modelled annual average concentrations of NO<sub>x</sub> and NO<sub>2</sub> in London in 2019; the left panels show results with (uncorrected) COPERT emissions factors, while the right panels show the relationship when using DUKEMS emissions factors. The solid line shows a 1:1 relationship, while the dotted lines represent ratios of 0.5 and 2 between modelled and measured data.

**Table 1**Road emissions of NO<sub>x</sub> and primary NO<sub>2</sub> by geographical zone in London, using different sets of emissions factors.

Location	COPERT		DUKEMS		Sensitivity		DUKEMS impact		Sensitivity impact	
	NO <sub>x</sub> (kt)	NO <sub>2</sub> (kt)	NO <sub>x</sub> (kt)	NO <sub>2</sub> (kt)	NO <sub>x</sub> (kt)	NO <sub>2</sub> (kt)	NO <sub>x</sub> (%)	NO <sub>2</sub> (%)	NO <sub>x</sub> (%)	NO <sub>2</sub> (%)
Central	0.60	0.09	0.92	0.14	0.92	0.14	53%	65%	0%	0%
Inner	6.15	0.91	8.48	1.25	8.47	1.25	38%	37%	0%	0%
Outer	10.95	1.62	15.05	2.17	14.95	2.16	38%	34%	-1%	-1%
External	3.33	0.48	4.41	0.62	4.30	0.61	32%	28%	-2%	-2%
M25	5.00	0.86	6.52	1.02	5.33	0.87	30%	18%	-18%	-14%
Total	26.02	3.96	35.38	5.20	33.96	5.03	36%	31%	-4%	-3%

The sensitivity test was conducted using COPERT emissions factors for heavy vehicles on road links with average speeds of above 80kph, and DUKEMS emissions factors elsewhere. The final two columns show the change in emissions in the sensitivity test relative to the run using DUKEMS emissions factors. Areas represented by each zone are illustrated in the supplementary material.

### 3.4. Air pollution model results

Fig. 7 and Table 2 show the air quality model performance using both updated DUKEMS emissions factors and those from COPERT for NO<sub>x</sub> and NO<sub>2</sub>. Annual average modelled concentrations are compared with those measured at 121 sites across the London area in 2019, and model performance statistics generated using the openair R package (Carslaw and Ropkins, 2012). Equivalent scatter plots and model statistics, broken down by geographical zone, are presented in the supplementary material.

The mean bias when using COPERT emissions factors in an uncorrected model is  $-4.5 \mu\text{g m}^{-3}$  for NO<sub>2</sub> and  $-14.5 \mu\text{g m}^{-3}$  for NO<sub>x</sub>. With the incorporation of the new curves in the road transport component of the emissions inventory, these figures change to  $+0.5 \mu\text{g m}^{-3}$  and  $+0.9 \mu\text{g m}^{-3}$  respectively. These changes equate to a reduction in the model's normalised mean bias, from  $-0.12$  to  $+0.01$  for NO<sub>2</sub> and from  $-0.18$  to  $+0.01$  for NO<sub>x</sub>.

The mean gross error is reduced, partly owing to this bias correction. However, the degree of scatter does not improve in the same way, decreasing slightly for NO<sub>x</sub>. The percentage of sites with a modelled concentration within a factor of 0.5 and 2 of the measurement site (FAC2) remains at 100% for NO<sub>2</sub>, while for NO<sub>x</sub> this value increases from 96% to 99%, with some underpredicted roadside sites brought within the FAC2 range. The coefficient of efficiency (COE) rises from 0.39 to 0.41 and from 0.42 to 0.49 for NO<sub>x</sub> and NO<sub>2</sub> respectively, illustrating improved model performance; this is also shown by corresponding increases in values of the closely related index of agreement (IOA).

## 4. Discussion

While discrepancies observed for individual vehicle types are more notable among HGVs and buses, those observed among both petrol and diesel light-duty vehicles contribute more substantially to the air pollution model overall. The effect of light-duty vehicle emissions changes on the model evaluation is more pronounced than is shown in Fig. 6, given that HGVs spend proportionally more of their time on larger roads beyond central and inner areas, in which there is a larger density of monitoring sites. Despite much recent focus on diesel vehicles, updates to petrol cars' emissions curves have a large impact on the model; this will become more important given ongoing trends away from diesel cars.

The discrepancies among diesel vehicles, including light and heavy-duty, ought to be considered in the context of colder ambient temperatures in the UK relative to the majority of European countries. The remote sensing data were collected at a mean temperature of 13.8 °C and at a minimum of  $-1$  °C, and ambient temperatures below 20 °C have been shown to increase NO<sub>x</sub> emissions from diesel cars because of reduction in the capability or deactivation of the vehicle's EGR system. Hausberger and Matzer reported that higher levels of condensation at lower ambient temperatures can severely compromise the system through processes including interlocking of the cooler or intake system, with the EGR rate reduced or deactivated in order to prevent damage (Hausberger and Matzer, 2017). A number of studies, using chassis dynamometer methods (Suarez-Bertoa and Astorga, 2018; Ko et al., 2017) and real-world measurements (Grange et al., 2019; Wærsted et al., 2022), have demonstrated such effects of ambient temperature. Using a Euro 6 light-duty diesel vehicle, Ko et al. reported NO<sub>x</sub> emissions at a 14 °C ambient temperature to be 2.5 and 2.8 times higher than those at 23 °C over the WLTC and NEDC respectively. These effects were even more substantial at the other test temperature of  $-5$  °C. The effects

**Table 2**Model performance statistics for NO<sub>x</sub> and NO<sub>2</sub> in London in 2019, with two different sets of road transport emissions factors.

Pollutant	Emissions Factors	<i>n</i>	FAC2	MB	MGE	NMB	NMGE	RMSE	<i>r</i>	COE	IOA
NO <sub>x</sub>	COPERT	121	0.96	-14.5	19.7	-0.18	0.24	28.1	0.81	0.39	0.69
	DUKEMS	121	0.99	0.9	19.1	0.01	0.24	28.3	0.80	0.41	0.70
NO <sub>2</sub>	COPERT	121	1.00	-4.5	5.9	-0.12	0.15	8.1	0.86	0.42	0.71
	DUKEMS	121	1.00	0.5	5.1	0.01	0.13	7.0	0.86	0.49	0.75

*n* = number of monitoring sites; FAC2 = fraction of predictions within a factor of 2; MB = Mean bias; MGE = Mean gross error; NMB = Normalised mean bias; NMGE = Normalised mean gross error; RMSE = Root mean squared error; *r* = Pearson correlation coefficient; COE = Coefficient of Efficiency; IOA = Index of Agreement.

were attributed to a decrease in the EGR valve open rate as temperature decreased, resulting from poor mixing of fuel and air, and reduced combustion efficiency and stability (Ko et al., 2017). Using the WLTC, Suarez-Bertoa and Astorga reported results consistent with those of Ko et al., through a comparison of ambient temperatures of  $-7$  and  $23$  °C across a group of five diesel vehicles (Suarez-Bertoa and Astorga, 2018).

Impacts of ambient temperature on the vehicle fleet as a whole were identified by Wærsted et al., who used measurement data from 2016 to 2019 at 46 roadside sites in Norway to generate an empirical  $\text{NO}_x$  correction factor of 2.7 across their inventory for ambient temperatures of  $-7$  °C, relative to temperatures above  $14$  °C (Wærsted et al., 2022).

In this study, the closer agreement with COPERT functions for Euro 6 diesel passenger cars, and the significantly higher emissions rates observed for Euro 3–5, may be explained by the results of Grange et al., who performed their analysis on some of the remote sensing dataset used in this study (Grange et al., 2019). They reported a weaker dependence on ambient temperature in Euro 6 relative to that in Euro 3–5. However, they also reported a very weak dependence of petrol vehicle emissions on ambient temperature, indicating that the discrepancies reported here among petrol cars are likely to be caused principally by other factors, such as underestimated degradation effects or a higher rate of failed catalytic converters than is being reported.

The effects of ambient temperature on emissions rates, distinct from the cold start emissions also discussed, ought to be considered in future emissions inventories. These could be utilized even more effectively with finer temporal resolution in the inventory, with ambient temperature used as an extra variable when producing emissions curves from remote sensing data such as that used in this study. This would remove the need to smooth out such effects when producing a single set of curves for an annual emissions estimate, which currently leads to some uncertainty.

The results indicate a large disparity between real-world emissions from Euro VI heavy vehicles and the curves currently recommended by EMEP. While the absolute discrepancies are greater for some Euro V HGVs, the overall impact of Euro VI discrepancies is greater in the 2019 emissions inventory in London; this impact will become relatively larger in emissions inventories for subsequent years.

The majority of the heavy vehicles whose measurements informed the production of the new speed-emissions curves were pre-Euro VI-D. The poor performance relative to that predicted by existing speed-emissions curves, and relative to the Euro VI standard, agrees with findings of Rodriguez, who summarised PEMS measurements of Euro VI HGVs (Rodriguez, 2020; Posada et al., 2020; Grigoratos et al., 2019). Notwithstanding the uncertainties at higher speeds, the results further highlight the poor performance of Euro VI HDVs under urban driving conditions. This is likely to be partly due to the well-documented decreased effectiveness of emission control systems under cold-start and low load operation (Rodriguez, 2020; Lyu et al., 2023).

The results could indicate failure or malfunctioning of, or tampering with, SCR systems on many of the vehicles sampled, and therefore within the vehicle fleet as a whole, given the scale of the discrepancy with existing speed-emissions curves under urban driving conditions. Testing of one HDV by Transport and Environment and the University of Graz found  $\text{NO}_x$  emissions 11 times higher than the Euro VI standard when the SCR system failed (Transport and Environment, 2021). The level of illegal tampering with HGVs, whereby the SCR system is turned off, is also something which has not been accurately quantified in the UK and will have a substantial impact on emissions from affected vehicles. Pöhler et al. conducted a plume-chasing campaign in Germany, Austria and Switzerland and reported that up to 25% of Euro VI HGVs may have been tampered with (Pöhler et al., 2019). Future emissions inventories would benefit from having an estimate of the scale of this problem.

The effectiveness of further iterations of the Euro VI standard cannot yet be evaluated using remote sensing data owing to limited data gathered since their implementation, but the recent inclusion of cold start testing in Euro VI-E is likely to have improved the new vehicles' performance (Rodriguez, 2020). A limited number of measurements from Euro VI heavy vehicles registered after 2018 have shown significantly lower emissions than prior iterations (approximately 60% lower). While this will have had minimal impact in 2019, such differences will be critical when using the data for future projections, and detailed policy scenario modelling for future years ought to include the latest data available.

The removal of the capping of the speed-emissions curves, at speeds below the typical thresholds of 5 kph and 10 kph as used in COPERT, resulted in some large increases in emissions on some links with very low average speeds in London. These low average speeds are rare, but do exist in very congested urban centres, particularly during the morning and evening peaks. Of the nearly 80,000 road links used in the model, 1.2% had at least one annual average hourly speed lower than the 5 kph threshold; however, none of these links were adjacent to a roadside or kerbside monitoring site location, so the performance of the model regarding this specific change could not be fully evaluated.

The results confirm that, despite discrepancies with COPERT, the newest (Euro 6-d) diesel cars and LGVs are performing substantially better than their predecessors with regard to  $\text{NO}_x$ , with lower emissions than the equivalent petrol vehicles at typical urban driving speeds. However, the fact that their primary  $\text{NO}_2$  emissions remain substantially higher in comparison to the petrol vehicles means that they will still contribute disproportionately to roadside  $\text{NO}_2$  concentrations.

The model performance upon adoption of the new speed-emissions curves, as shown in Fig. 7 and Table 2, is greatly improved when compared with that when using the COPERT curves currently recommended by EMEP. While the model's bias is greatly reduced, there is not a significant reduction in scatter; it is important to stress that the degree of scatter will always be difficult to control given other assumptions in the model, in addition to the uncertainties in the emissions factors discussed. The model necessarily simplifies the dispersion in what are in reality very complex environments; each road link also in reality has unique characteristics including vehicle fleet composition and traffic flow behaviour, which the zonal fleet compositions, annually averaged traffic and speed data available ultimately cannot fully capture.

#### 4.1. Uncertainties

Average speed is a relatively poor predictor of emission rate, with the absolute range of uncertainty in predicted emission rates growing at higher average speeds. Future emissions inventories would benefit from the presence of other metrics measured at road link level which better quantify driving behaviour and typical vehicle-specific power. There is an opportunity for emerging datasets involving GPS tracking of vehicles to improve emissions inventories by removing the dependence on average speed as a predictor, if there was sufficient coverage across roads within an urban area. Road links represented in urban emissions inventories are typically bi-directional, with one average speed assumed for both sides of the road. Given the disparities in emissions observed under acceleration and deceleration at a given average speed, further work could improve emissions estimates by better characterizing levels of acceleration and deceleration on such road links, while making use of the same dataset used in this study.

Further work could benefit from more specific measurements from different bus technologies; there is uncertainty around the assumptions on hybrid buses, and within the subset of hybrid buses, emissions rates are complex (Phantawesak et al., 2022).

The lack of sufficient measured data from coaches, petrol LGVs, and for several weight classes of articulated HGV, meant new curves were not fitted for these; further iterations would benefit from more measurements from these vehicles.

Cold start emissions from light-duty vehicles were accounted for in addition to the curves used, since the remote sensing measurements were assumed to represent hot emissions only. Any measurements of light-duty vehicles which represented emissions under cold start conditions will have contributed to an overestimation in emissions by the new methods. With regard to the cold emissions rates from heavy vehicles estimated using the COPERT functions, the proportion of time spent under these operating conditions, having been set at 100% on road links below the speed threshold, could be overestimated; if so, the discrepancies with the new speed-emissions curves would increase further at these speeds.

The application of the remote sensing data to future projections has more uncertainty associated with it, given that the measurements were made from 2017 to 2022 and therefore accounted for the degradation observed in the respective euro standards over that period. Older vehicles persisting in the fleet would be expected to degrade further in future years and consequently have higher emissions; this further emphasises the need for ongoing measurement campaigns to monitor the effects of degradation on more recently registered vehicles.

## 5. Conclusions

This study has demonstrated a methodology for development of speed-emissions curves using remote sensing data and available vehicle drive cycles, incorporating new data including that from heavy vehicles. Crucially, it has also now been demonstrated that these can be applied in a detailed emissions inventory and led to substantially improved air pollution model performance. NO<sub>x</sub> emissions from road transport increased by 36% across the whole model area, leading to the normalised mean bias in the model reducing from  $-0.18$  to  $+0.01$  for NO<sub>x</sub> and  $-0.12$  to  $+0.01$  for NO<sub>2</sub>. The correction of the bias in the air pollution model furthers the case for the adoption of such curves in national and city-level emissions inventories. This would lead to revision of NO<sub>x</sub> emissions budgets when evaluating compliance with the NEC Directive, and could greatly improve future model predictions as well as providing more accurate data for health-related exposure studies. The discrepancies between the new curves and the existing ones highlight a challenge for manufacturers and policymakers in continuing to reduce NO<sub>2</sub> concentrations at urban roadside locations with existing vehicle technologies, particularly in colder climates. Adoption of the new curves would better enable the development of new and specific policies to focus on mitigating the impact of particularly polluting vehicles.

Further revisions to these curves are recommended, to account fully for further iterations to Euro standards and test procedures, as well as vehicle degradation and the effects of ambient temperature, which will have varying impacts in different countries. National-level inventories, which will be influenced more by motorway driving, would benefit from further remote sensing data measured at high speed from heavy-duty diesel vehicles. These steps will all be important in evaluating the effectiveness of net-zero emissions targets, as well as Clean Air Zones such as those recently implemented in the UK, on reducing air pollution in years to come.

## Funding sources

This research was funded by the UK National Environment Research Council (NERC) and the UK Met Office through the DUKEMS (Developing a UK Community Emission Modelling System) project (CA19-3), which was part of the UKRI SPF Clean Air Programme. We also thank the National Institute for Health Research (NIHR) for funding of the PHR Project: NIHR129406 “The air quality health and economic costs and benefits of a zero carbon UK”.

This study was part-funded by the National Institute for Health Research (NIHR) Health Protection Research Unit in Environmental Exposures and Health, a partnership between the UK Health Security Agency and Imperial College London. The views expressed are those of the authors and not necessarily those of the NIHR and UK Health Security Agency.

## CRedit authorship contribution statement

**Gregor B. Stewart:** Conceptualization, Methodology, Formal analysis, Investigation, Visualization, Writing – original draft, Writing – review & editing. **David Dajnak:** Conceptualization, Methodology, Formal analysis, Investigation, Writing – review & editing. **Jack Davison:** Methodology, Formal analysis, Investigation. **David C. Carslaw:** Conceptualization, Methodology, Formal analysis, Investigation, Writing – review & editing, Funding acquisition. **Andrew V. Beddows:** Methodology, Formal analysis.

**Napameth Phantawesak:** Formal analysis. **Marc E.J. Stettler:** Formal analysis, Funding acquisition. **Michael J. Hollaway:** Funding acquisition, Supervision. **Sean D. Beevers:** Conceptualization, Methodology, Formal analysis, Writing – review & editing, Funding acquisition, Supervision.

### Declaration of competing interest

The authors declare that they have no known competing financial interests or personal relationships that could have appeared to influence the work reported in this paper.

### Data availability

Some of the data used or produced may be available on request

### Acknowledgements

The authors thank the UK National Environment Research Council (NERC) and the Met Office for funding the DUKEMS project (Developing a UK Community Emissions Modelling System) through the Strategic Priorities Fund (SPF) Clean Air Programme. We thank Transport for London for provision of road traffic flows, speeds and vehicle fleet compositions used to undertake the London Atmospheric Emissions Inventory 2019, and further applied in this research. We also thank Transport for London, as well as the Energy Saving Trust and Zemo, for the drive cycle data used.

### Appendix A. Supplementary data

Supplementary data to this article can be found online at <https://doi.org/10.1016/j.uclim.2024.102103>.

### References

- Aether Ltd, 2017. Port of London Emissions Inventory 2016. Report to Port of London Authority and Transport for London. cited 2021; Available from: <https://server2.pla.co.uk/assets/finalplaportwideinventoryoutputsreportv10.2publication.pdf>.
- Beekmann, M., et al., 2015. In situ, satellite measurement and model evidence on the dominant regional contribution to fine particulate matter levels in the Paris megacity. *Atmos. Chem. Phys.* 15 (16), 9577–9591. <https://doi.org/10.5194/acp-15-9577-2015>.
- Beevers, S.D., et al., 2012. One way coupling of CMAQ and a road source dispersion model for fine scale air pollution predictions. *Atmos. Environ.* 59 (C), 47–58. <https://doi.org/10.1016/j.atmosenv.2012.05.034>.
- Beevers, S.D., et al., 2013. Air pollution dispersion models for human exposure predictions in London. *J. Expo. Sci. Environ. Epidemiol.* 23 (6), 647–653. <https://doi.org/10.1038/jes.2013.6>.
- Bishop, G.A., Stedman, D.H., 1996. Measuring the emissions of passing cars. *Acc. Chem. Res.* 29 (10), 489–495. <https://doi.org/10.1021/ar950240x>.
- Bishop, J.D.K., Molden, N., Boies, A.M., 2019. Using portable emissions measurement systems (PEMS) to derive more accurate estimates of fuel use and nitrogen oxides emissions from modern euro 6 passenger cars under real-world driving conditions. *Appl. Energy* 242, 942–973. <https://doi.org/10.1016/j.apenergy.2019.03.047>.
- Burgard, D.A., et al., 2006. Spectroscopy applied to on-road Mobile source emissions. *Appl. Spectrosc.* 60 (5), 135A–148A. <https://doi.org/10.1366/000370206777412185>.
- Byun, D., Schere, K.L., 2006. Review of the governing equations, computational algorithms, and other components of the Models-3 community multiscale air quality (CMAQ) modeling system. *Appl. Mech. Rev.* 59 (2), 51–77. <https://doi.org/10.1115/1.2128636>.
- Cambridge Environmental Research Consultants, 2016. *ADMS 5 Atmospheric Dispersion Modelling System User Guide, Version 5.2*.
- Cambridge Environmental Research Consultants, 2020. *ADMS-Roads Air Quality Management System User Guide, Version 5.0*.
- Carlsaw, D., 2023. worldmet: Import Surface Meteorological Data from NOAA Integrated Surface Database (ISD). R package version 0.9.7. Available from: <https://CRAN.R-project.org/package=worldmet>.
- Carlsaw, D.C., Rhys-Tyler, G., 2013. New insights from comprehensive on-road measurements of NO<sub>x</sub>, NO<sub>2</sub> and NH<sub>3</sub> from vehicle emission remote sensing in London, UK. *Atmos. Environ.* 81, 339–347. <https://doi.org/10.1016/j.atmosenv.2013.09.026>.
- Carlsaw, D.C., Ropkins, K., 2012. Openair — an R package for air quality data analysis. *Environ. Model Softw.* 27–28, 52–61. <https://doi.org/10.1016/j.envsoft.2011.09.008>.
- Carlsaw, D.C., Beevers, S.D., Fuller, G., 2001. An empirical approach for the prediction of annual mean nitrogen dioxide concentrations in London. *Atmos. Environ.* 35 (8), 1505–1515. [https://doi.org/10.1016/S1352-2310\(00\)00287-9](https://doi.org/10.1016/S1352-2310(00)00287-9).
- Carlsaw, D.C., et al., 2011. Recent evidence concerning higher NO<sub>x</sub> emissions from passenger cars and light duty vehicles. *Atmos. Environ.* 45 (39), 7053–7063. <https://doi.org/10.1016/j.atmosenv.2011.09.063>.
- Carlsaw, D.C., et al., 2013. The importance of high vehicle power for passenger car emissions. *Atmos. Environ.* 68, 8–16. <https://doi.org/10.1016/j.atmosenv.2012.11.033>.
- Casquero-Vera, J.A., et al., 2019. Impact of primary NO<sub>2</sub> emissions at different urban sites exceeding the European NO<sub>2</sub> standard limit. *Sci. Total Environ.* 646, 1117–1125. <https://doi.org/10.1016/j.scitotenv.2018.07.360>.
- Chen, Y., Borken-Kleefeld, J., 2016. NO<sub>x</sub> emissions from diesel passenger cars worsen with age. *Environ. Sci. Technol.* 50 (7), 3327–3332. <https://doi.org/10.1021/acs.est.5b04704>.
- Clappier, A., et al., 2021. Impact of SO<sub>x</sub>, NO<sub>x</sub> and NH<sub>3</sub> emission reductions on PM<sub>2.5</sub> concentrations across Europe: hints for future measure development. *Environ. Int.* 156, 106699 <https://doi.org/10.1016/j.envint.2021.106699>.
- Dajnak, D., et al., 2023. Can the UK meet the World Health Organization PM<sub>2.5</sub> interim target of 10 µg m<sup>-3</sup> by 2030? *Environ. Int.* 181, 108222 <https://doi.org/10.1016/j.envint.2023.108222>.
- Davison, J., et al., 2020. Distance-based emission factors from vehicle emission remote sensing measurements. *Sci. Total Environ.* 739, 139688 <https://doi.org/10.1016/j.scitotenv.2020.139688>.

- Davison, J., et al., 2021. Verification of a National Emission Inventory and influence of on-road vehicle manufacturer-level emissions. *Environ. Sci. Technol.* 55 (8), 4452–4461. <https://doi.org/10.1021/acs.est.0c08363>.
- Department for Transport, 2009. Mileage Fuel Scaling Factors. ; Available from: <https://www.gov.uk/government/publications/road-vehicle-emission-factors-2009>. Emisia. COPERT (2023). ; Available from: <https://www.emisia.com/utilities/copert/>.
- European Environment Agency, 2019. *EMEP/EEA Air Pollutant Emission Inventory Guidebook 2019 - Update Oct. 2021*.
- European Environment Agency, 2022. Sources and Emissions of Air Pollutants in Europe. Updated 01 Dec 2022 [24/11/23]; Available from: <https://www.eea.europa.eu/publications/air-quality-in-europe-2022/sources-and-emissions-of-air>.
- European Environment Agency, 2023. *Europe's Air Quality Status 2023*, 31st May 2023 24/11/23]; Available from: <https://www.eea.europa.eu/publications/europes-air-quality-status-2023>.
- Farren, N.J., et al., 2020. Underestimated ammonia emissions from road vehicles. *Environ. Sci. Technol.* 54 (24), 15689–15697. <https://doi.org/10.1021/acs.est.0c05839>.
- Garland, L., et al., 2022. Air Pollutant Inventories for England, Scotland, Wales, and Northern Ireland: 2005-2020. [https://naei.beis.gov.uk/reports/reports?report\\_id=1100](https://naei.beis.gov.uk/reports/reports?report_id=1100). Available from.
- Grange, S.K., et al., 2019. Strong temperature dependence for light-duty diesel vehicle NO<sub>x</sub> emissions. *Environ. Sci. Technol.* 53 (11), 6587–6596. <https://doi.org/10.1021/acs.est.9b01024>.
- Greater London Authority, 2021. *London Atmospheric Emissions Inventory (LAEI) 2019*. August 1, 2022]; Available from: <https://data.london.gov.uk/dataset/london-atmospheric-emissions-inventory-laei-2019>.
- Grigoratos, T., et al., 2019. Real world emissions performance of heavy-duty euro VI diesel vehicles. *Atmos. Environ.* 201, 348–359. <https://doi.org/10.1016/j.atmosenv.2018.12.042>.
- Hausberger, S., 2003. Simulation of Real World Vehicle Exhaust Emissions. Technische Universität Graz, Austria.
- Hausberger, S., Matzer, C., 2017. Update of Emission Factors for EURO 4, EURO 5 and EURO 6 Diesel Passenger Cars for the HBEFA Version 3.3. Report No. I-09/17/CM EM 16/26/679. Graz University of Technology.
- Heathrow Airport Ltd, et al., 2023. Heathrow Airwatch. cited. Available from: <http://www.heathrowairwatch.org.uk/>.
- Imperial College London, 2023. London Air Quality Network. cited. Available from: <https://www.londonair.org.uk/>.
- Kelly, F., et al., 2011. The impact of the congestion charging scheme on air quality in London. Part 1. Emissions modeling and analysis of air pollution measurements. *Res. Rep. Health Eff. Inst.* 155, 5–71.
- Ko, J., et al., 2017. Comparative investigation of NO<sub>x</sub> emission characteristics from a euro 6-compliant diesel passenger car over the NEDC and WLTC at various ambient temperatures. *Appl. Energy* 187, 652–662. <https://doi.org/10.1016/j.apenergy.2016.11.105>.
- Lewis, A.C., Carslaw, D.C., Kelly, F.J., 2015. Vehicle emissions: diesel pollution long under-reported. *Nature* 526 (7572), 195. <https://doi.org/10.1038/526195c>.
- Lyu, L., et al., 2023. NO<sub>x</sub> emission deterioration in modern heavy-duty diesel vehicles based on long-term real driving measurements. *Environ. Res.* 232, 116396 <https://doi.org/10.1016/j.envres.2023.116396>.
- Murrells, T., Rose, R., 2019. Production of Updated Emission Curves Use in the NTM and WebTAG SPaTS. Work Package 1650. Report for the Department for Transport.
- National Atmospheric Emissions Inventory, 2022 [cited 2023 24/11/23]; Available from: <https://naei.beis.gov.uk/data/ef-transport>.
- Notter, B., et al., 2022. HBEFA 4.2 - Documentation of Updates. Available from: [https://assets-global.website-files.com/6207922a2acc01004530a67e/6217584903e9f9b63093c8c0\\_HBEFA42\\_Update\\_Documentation.pdf](https://assets-global.website-files.com/6207922a2acc01004530a67e/6217584903e9f9b63093c8c0_HBEFA42_Update_Documentation.pdf).
- Ntziachristos, L., Samaras, Z., 2023. *Sectoral Guidance 1.A.3.b Road Transport. EMEP/EEA Air Pollutant Emission Inventory Guidebook 2019–2023 Update*. European Environment Agency.
- O'Driscoll, R., et al., 2016. A portable emissions measurement system (PEMS) study of NO<sub>x</sub> and primary NO<sub>2</sub> emissions from euro 6 diesel passenger cars and comparison with COPERT emission factors. *Atmos. Environ.* 145, 81–91. <https://doi.org/10.1016/j.atmosenv.2016.09.021>.
- O'Driscoll, R., et al., 2018. Real world CO<sub>2</sub> and NO<sub>x</sub> emissions from 149 euro 5 and 6 diesel, gasoline and hybrid passenger cars. *Sci. Total Environ.* 621, 282–290. <https://doi.org/10.1016/j.scitotenv.2017.11.271>.
- Ordnance Survey, 2023. OS Open TOID. ; Available from: <https://www.ordnancesurvey.co.uk/products/os-open-toid>.
- Phantawesak, N., Coyle, F., Stettler, M.E.J., 2022. Long-term in-use NO<sub>x</sub> emissions from London buses with retrofitted NO<sub>x</sub> Aftertreatment. *Environ. Sci. Technol.* 56 (11), 6968–6977. <https://doi.org/10.1021/acs.est.1c05083>.
- Pöhler, D., et al., 2019. Real driving NO<sub>x</sub> emissions and emission manipulations of trucks observed with plume chasing. *Geophys. Res. Abstr.* 21. EGU2019-14317-1. <https://meetingorganizer.copernicus.org/EGU2019/EGU2019-14317-1.pdf>.
- Port of London Authority, 2022. Personal Communication.
- Posada, F., Badshah, Huzeifa, Rodriguez, F., 2020. ICCT White Paper: In-Use NO<sub>x</sub> Emissions and Compliance Evaluation for Modern Heavy-Duty Vehicles in Europe and the United States. Available from: <https://theicct.org/publication/in-use-nox-emissions-and-compliance-evaluation-for-modern-heavy-duty-vehicles-in-europe-and-the-united-states/>.
- Ricardo Energy & Environment, 2023. Air Quality England. cited. Available from: <https://www.airqualityengland.co.uk/>.
- Rodriguez, F., 2020. International Council on Clean Transportation Briefing: Commercial Fleet Renewal Programs as a Response to the COVID-19 Crisis in the European Union. Available from: <https://theicct.org/publication/commercial-fleet-renewal-programs-as-a-response-to-the-covid-19-crisis-in-the-european-union/>.
- Söderena, P., et al., 2020. Monitoring euro 6 diesel passenger cars NO<sub>x</sub> emissions for one year in various ambient conditions with PEMS and NO<sub>x</sub> sensors. *Sci. Total Environ.* 746, 140971 <https://doi.org/10.1016/j.scitotenv.2020.140971>.
- Suarez-Bertoa, R., Astorga, C., 2018. Impact of cold temperature on euro 6 passenger car emissions. *Environ. Pollut.* 234, 318–329. <https://doi.org/10.1016/j.envpol.2017.10.096>.
- Transport and Environment, 2021. Euro VI Trucks Still Don't Meet Emission Limits on the Road. Available from: [https://www.transportenvironment.org/wp-content/uploads/2021/11/2021\\_11\\_Euro\\_VII\\_HD\\_policy\\_paper\\_2021.pdf](https://www.transportenvironment.org/wp-content/uploads/2021/11/2021_11_Euro_VII_HD_policy_paper_2021.pdf).
- UK Department for Energy Security and Net Zero and UK Department for Business Energy and Industrial Strategy, 2024. Gas Stat. ; Available from: <https://www.gov.uk/government/collections/gas-statistics>.
- United States Environmental Protection Agency, 2022. CMAQ (Version 5.4). Available from: <https://doi.org/10.5281/zenodo.7218076>.
- Wærsted, E.G., et al., 2022. Quantification of temperature dependence of NO<sub>x</sub> emissions from road traffic in Norway using air quality modelling and monitoring data. *Atmos. Environ.* 13, 100160 <https://doi.org/10.1016/j.aeoa.2022.100160>.
- Wood, S.N., 2017. *Generalized Additive Models: An Introduction with R*. CRC press.
- Zheng, X., et al., 2021. Real-time black carbon emissions from light-duty passenger vehicles using a portable emissions measurement system. *Engineering*. <https://doi.org/10.1016/j.eng.2020.11.009>.